Linking contrast sensitivity to cortical magnification in human primary visual cortex

Marc M. Himmelberg[1,2], Jonathan Winawer[^1,2] & Marisa Carrasco[^1,2]

Affiliations:
[1] Department of Psychology, New York University, New York, NY, USA, 10003
[2] Center for Neural Science, New York University, New York, NY, USA, 10003
[^] Equal contributors

Corresponding Author: Marc Himmelberg, Department of Psychology, 6 Washington Place, New York University, NY, 10003 (marc.himmelberg@nyu.edu)

Competing Interest Statement: The authors declare no competing financial interests.

Classification: Biological Sciences; Neuroscience

Keywords: cortical magnification, contrast sensitivity, retinotopy, visual performance fields, individual differences

ABSTRACT

The size and organization of primary visual cortex (V1) varies across individuals. Across neurotypical adults, V1 size varies more than twofold. Within individuals, surface area per unit of visual field – cortical magnification – varies with eccentricity and polar angle. Contrast sensitivity and cortical magnification covary with eccentricity, therefore it has been hypothesized that cortical magnification, specifically the number of activated V1 neurons, limits contrast sensitivity. Here, we quantify the relation between contrast sensitivity and V1 cortical magnification across observers and polar angle. We measured contrast sensitivity at four cardinal meridians in 29 observers. We then used fMRI to measure the size of V1 in the same observers, and the amount of surface area representing each of the four meridians (wedge-ROIs within 15° polar angle of the meridians, 1 to 8° eccentricity). We found that: First, an observer's contrast sensitivity (averaged across polar angles) was predicted by the size of V1. Second, contrast sensitivity at each cardinal meridian was correlated with the surface area of the wedge-ROIs centered at the corresponding meridian. Third, increases in contrast sensitivity and cortical magnification at the horizontal compared to vertical meridian (horizontal-vertical anisotropy, 'HVA') were strongly correlated: a larger HVA in contrast sensitivity corresponded to a larger HVA in cortical magnification. These results reveal that contrast sensitivity and cortical magnification co-vary across observers and demonstrate a link between perceptual polar angle asymmetries and cortical anatomy. Broadly, the results show a link between visual perception and the idiosyncratic cortical organization of V1 in neurotypical observers.

SIGNIFICANCE STATEMENT

Contrast sensitivity is a fundamental property of the human visual system, which indexes the limits of what one can detect or discriminate – the window of visibility. Contrast sensitivity varies with stimulus location on the retina and across observers. These variations are not well understood. Using psychophysics and magnetic resonance imaging, we tested the hypothesis that contrast sensitivity depends on the amount of responsive tissue in primary visual cortex (V1). Individuals with greater contrast sensitivity had a larger V1. Further, within observers, variation in contrast sensitivity across polar angle locations matched the variation in V1 surface area representing those locations. These findings demonstrate a tight link between visual perception and cortical anatomy, both within and among people.

INTRODUCTION

The size and organization of human primary visual cortex (V1) varies across individuals. V1 surface area varies more than twofold across individuals, even in the adult neurotypical population (1–4). V1 surface area also varies within individuals. Specifically, the amount of V1 tissue dedicated to processing a fixed spatial extent on the retina (*cortical magnification*) changes sharply as a function of eccentricity and polar angle (5–9). Moreover, within- and between-subject variation interact: even after accounting for differences in overall V1 size between observers, the cortical magnification functions for eccentricity and polar angle vary across individuals (3, 8).

Variation in cortical magnification has important consequences for visual perception. In human and non-human primates, visual performance is best near the fovea and decreases with increasing eccentricity. This is reflected in the cortical magnification function, in which V1 surface area is greatest at the fovea and decreases with increasing eccentricity (2, 5, 7, 9–12). Visual performance also changes as a function of polar angle; it is better along the horizontal than vertical meridian (horizontal-vertical anisotropy, HVA), and along the lower than upper vertical meridian (vertical meridian asymmetry, VMA) (13–19). These perceptual polar angle asymmetries have been linked to similar asymmetries in V1 cortical magnification: in humans and macaque monkey, more local V1 surface area is dedicated to processing the horizontal than vertical meridian (i.e., a cortical HVA), and the lower than upper vertical meridian (i.e., a cortical VMA) (6–8, 20). Furthermore, polar angle asymmetries in cortical magnification are at least in part heritable – the magnitudes of the asymmetries are more similar for monozygotic than dizygotic twins (8). Individual variation in V1 cortical magnification (both the total size of V1 and how its surface area is distributed across the visual field map) may account for individual differences in visual perception.

Contrast is the currency of the visual system, driving neural and perceptual responses for most, if not all, visual tasks. V1 neurons are highly sensitive to contrast (21–25), with their firing rates reaching half of their maximal response (c_{50}) at contrasts as low as ~4% (21, 26). Contrast sensitivity and cortical magnification co-vary as a function of eccentricity (i.e., contrast sensitivity and cortical magnification *decrease* with *increasing* eccentricity) (27). A possible linking hypothesis connecting these two observations is that contrast sensitivity is determined by the number of activated V1 neurons (27). As the cytoarchitecture of V1 is approximately uniform (28, 29), portions of V1 with substantially more dedicated cortical surface area per square degree of visual field should also have more neurons, and contrast sensitivity at some location in the visual field should increase in proportion to the amount of dedicated cortical surface area, thereby linking contrast sensitivity with cortical magnification.

This linking hypothesis was originally proposed to explain changes in contrast sensitivity as a function of eccentricity. Here, we extend this logic to individual variation in V1 size, and to local measurements of V1 surface area taken as a function of polar angle, across observers.

To assess the link between contrast sensitivity and cortical magnification, observers completed an orientation discrimination task to measure contrast sensitivity at the four polar angle meridians in the visual field (left and right horizontal, upper vertical, and lower vertical). In the same observers, we then used an fMRI retinotopic mapping experiment to delineate V1 maps. We calculated the V1 surface area (out to 8° eccentricity), and the surface area of 'wedge ROIs', defined as the portions of V1 dedicated to processing ±15° regions of the visual field centered along the same four meridians as in the contrast sensitivity measurements. As the wedge-ROIs always represent the same size region of visual space (±15° of polar angle, 1 to 8° of eccentricity), any differences in V1 surface area measurements derived from the wedge-ROIs can be considered to index differences in cortical magnification.

Specifically, we asked:

1. Is there a correlation between contrast sensitivity (averaged across polar angle location) and the overall size of V1?
2. Is there a correlation between local contrast sensitivity and local V1 surface area measurements (i.e., cortical magnification), taken from different polar angle locations?
3. Is there a correlation between polar angle asymmetries in contrast sensitivity (i.e., the behaviorally defined HVA and VMA) and polar angle asymmetries in V1 surface area (i.e., the cortically defined HVA and VMA)?

RESULTS

V1 size varies substantially across observers

First, we assessed the distribution of V1 surface area across 29 observers. Here, we report V1 surface area per hemisphere, from 0° to 8° eccentricity, which comprises almost half of V1. We limit the range to 8° because the functional data are less reliable near the edge of the retinotopic mapping stimulus (12.4°). Consistent with previous reports, the surface area of V1 varied ~two-fold (specifically by 110%, the largest V1 being 1,746 mm^2 and the smallest being 829 mm^2) (**Figure 1A**). The variability in V1 surface area is substantial, especially when compared to the total surface area of the cortex (**Figure 1B**), which varied by 50% (the largest hemisphere of the cortex being 0.12m^2 and the smallest being 0.08m^2). **Figure 1D** shows visualizations of polar angle and eccentricity maps from the left V1 for the largest and smallest V1s. Both had clear, full representations of the right visual hemifield, indicating that the visual field maps were clear and complete, and there were no errors in delineating their boundaries. Instead, the retinotopic representations are simply compressed for the observer with smaller V1. These large individual differences are not a result of biological sex differences. In fact, we found little difference in the size of V1 between females and males, regardless of whether we normalize the size of V1 to total cortical surface area: ($p > .1$ for both comparisons, unpaired two-tailed t-tests).

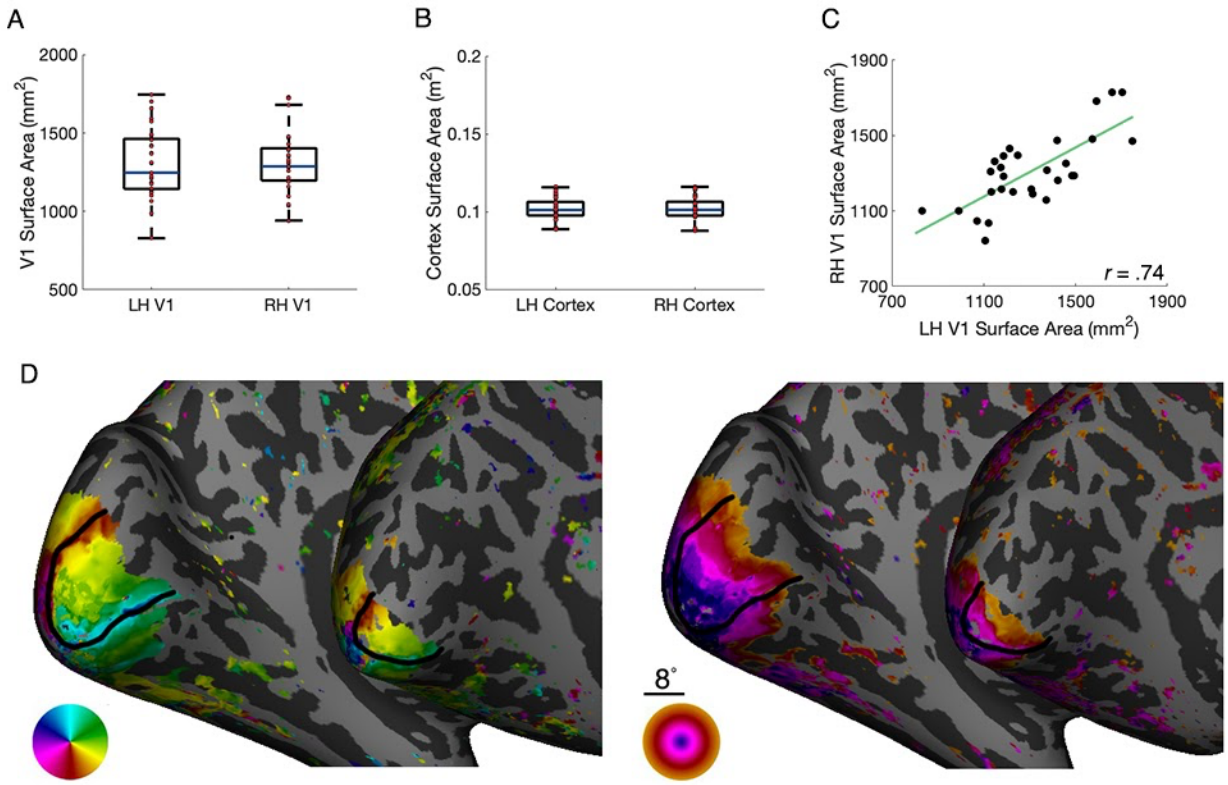

Figure 1. (A) Surface area (mm^2) for the left and right hemispheres of V1 and **(B)** the total surface area for left and right hemispheres of the cortex (n=29). The y-axes are matched so that the scaling in **(B)** is 4x the size of that in panel **(A)**. Individual data are plotted in red. Top and bottom edges of each box represent the 75th and 25th percentiles, respectively. The whiskers extend to most extreme data points not considered outliers. **(C)** The surface area of the left and right hemispheres of V1 is strongly correlated within observers (r_ρ = .74, p < .001). **(D)** Polar angle and eccentricity maps on the inflated left hemisphere for the observers with the largest and smallest V1s. The border of V1 is defined by the black lines and data are shown out to 8° of eccentricity.

Although V1 surface area varies *across* individuals, previous reports show that the surface areas of left and right V1 are relatively similar *within* individuals (1, 2, 4). Here, too, we found that the surface area of left and right V1 were highly correlated (r = .74, p < .001, **Figure 1C**).

Group-level polar angle asymmetries for contrast sensitivity and V1 surface area

We tested whether the expected polar angle asymmetries existed in our behavioral and cortical data at the group level and calculated a summary metric to describe the strength of these asymmetries. First, to calculate contrast sensitivity along the horizontal meridian, we averaged contrast sensitivity measurements from the left and right horizontal meridians. Similarly, to calculate contrast sensitivity along the vertical meridian, we averaged together contrast sensitivity measurements from the upper and lower vertical meridians. To calculate the amount of V1 surface area dedicated to processing the horizontal meridian, surface area measurements from the wedge-ROIs centered on the left and right horizontal meridians were summed. Similarly, to calculate the surface area of the vertical meridian, the V1 surface area measurements of

wedge-ROIs centered on the upper and lower vertical meridian were summed. See Methods section *Defining wedge-ROIs* for further details.

We also calculated an asymmetry index value as a summary metric for the horizontal-vertical anisotropy (HVA; the asymmetry between the horizontal and vertical meridian) and the vertical meridian asymmetry (VMA; the asymmetry between the lower and upper vertical meridian), for both contrast sensitivity and V1 surface area. The HVA index was calculated as the difference in contrast sensitivity (or local V1 surface area) between the horizontal and vertical meridian, divided by the mean of the two, multiplied by 100. The VMA index was calculated as the difference in contrast sensitivity (or local V1 surface area) between the lower and upper vertical meridian, divided by the mean of the two, multiplied by 100.

As expected, there were both an HVA and VMA at the group-level in our contrast sensitivity data. Contrast sensitivity was significantly greater at the horizontal than the vertical meridian (HVA) ($t(28) = 16.88$, $p < .001$, $d = 2.95$; paired samples t-test; **Figure 2A**) with a mean HVA index of 39%. Contrast sensitivity was greater at the lower vertical than the upper vertical meridian (VMA) ($t(28) = 4.18$, $p < .001$, $d = .78$; **Figure 2A**), with a mean VMA index of 13%. Likewise, we confirmed the HVA and VMA at the group-level in the V1 surface area data. There was significantly more V1 surface area dedicated to the horizontal than vertical meridian (HVA) ($t(28) = 16.23$, $p < .001$, $d = .31$; **Figure 2B**), with a mean cortical HVA index of 59%. There was more V1 surface area dedicated to the lower vertical than upper vertical meridian (VMA) ($t(28) = 2.82$, $p < .01$, $d = .52$; **Figure 2B**), with a mean cortical VMA index of 25%. Note that there was neither a main effect of biological sex nor did it interact with location (HVA or VMA) for contrast sensitivity or surface area ($p > .1$ for main effects of biological sex and interactions; 2x 2-way (2 locations x 2 biological sexes) repeated measures ANOVAs).

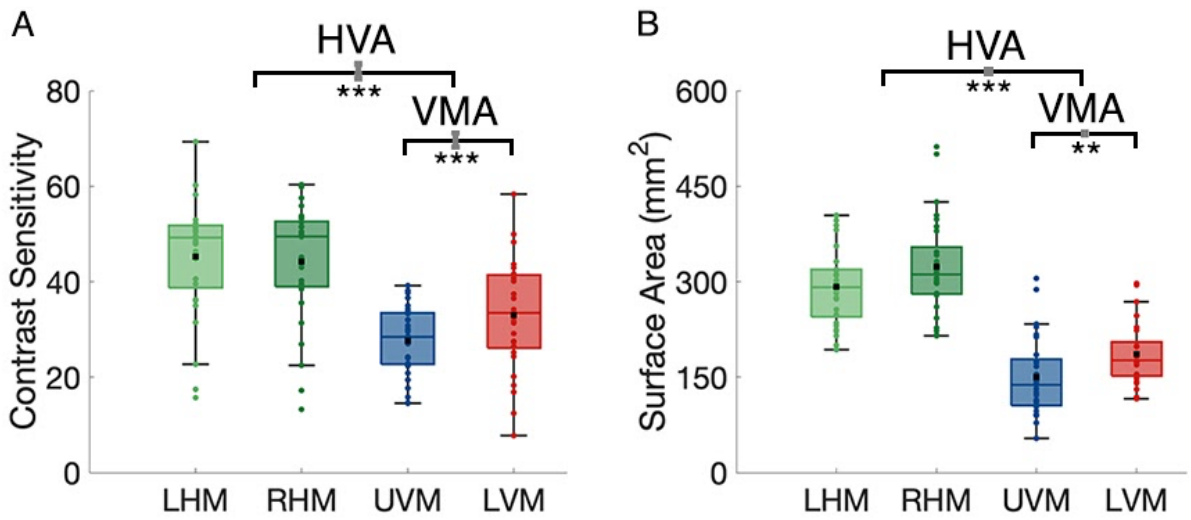

Figure 2. (A) Group-level contrast sensitivity measurements from the four polar angle meridians and **(B)** group-level V1 surface area measurements from wedge-ROIs (±15°) centered on the four polar angle meridians (n=29). Colored data points indicate individual measurements. The black datapoint represents the group average and the colored horizontal line represents the group median. Grey error bars on the horizontal brackets represent ±1 standard error of the difference. Top and bottom edges of each box represent the 75th and 25th percentiles, respectively. The whiskers extend to most extreme data points not considered outliers. ** $p < .01$, *** $p < .001$.

Additionally, we identified slightly more V1 surface area dedicated to the right than the left horizontal meridian ($p < .05$, $d = .48$). In a supplementary analysis we tested this left-right horizontal meridian asymmetry using an extended dataset (n=54; the 29 observers here, as well as 25 more who had retinotopy measurements but no psychophysics data) and found that this slight bias for more surface area along the right than left horizontal meridian held ($p < .05$, $d = .28$; **Figure S1**).

Quantifying the relation between contrast sensitivity and overall V1 surface area.

After confirming the polar angle asymmetries in our group-level data, we measured the relation between contrast sensitivity and V1 surface area at different scales, across individual observers. The relation between these two variables is non-linear; an increase in V1 surface area does not necessarily correspond to a proportional increase in contrast sensitivity. However, the relation between these two variables is hypothesized to be monotonic and positive; as surface area increases, so will contrast sensitivity. Thus, the following analyses were assessed using one-tailed Spearman's rho; r_ρ (30).

First, we asked whether contrast sensitivity averaged across the four polar angle locations correlated with overall surface area, and thus size, of V1 (summed across hemispheres, and restricted to 0 to 8° of eccentricity). Averaged contrast sensitivity across location and was positively correlated with V1 surface area ($r_\rho = .45$, $p < .01$; **Figure 3**). The surface area of a cortical region depends on the cortical depth used to define the surface. The superficial surface (boundary of gray and white matter) will have an overall larger surface area than a surface defined

at a deeper layer (gray/white matter boundary). Moreover, the superficial layer will be biased to have greater surface area for gyri and the deeper surfaces will be biased to have greater surface area for sulci. To reduce these biases, we defined surface area on the midgray surface, half-way between the white matter and the pial surface. As a further check, we also measured all effects relative to the white matter surface and the pial surface, with no major change in the pattern of results. A significant correlation was found when V1 surface area was calculated using the pial (**Figure S2A**) or white matter (**Figure S2B**) surfaces, rather than the midgray (see Methods: *Defining wedge-ROIs*). Observers with a larger V1 tended to have relatively greater contrast sensitivity, whereas those with a smaller V1 tended to have lower contrast sensitivity.

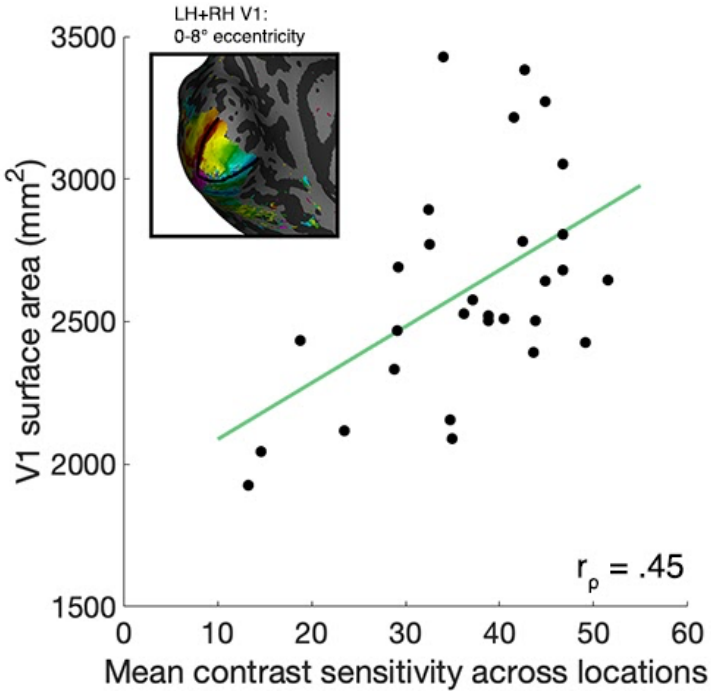

Figure 3. Average contrast sensitivity across polar angle locations correlates with V1 surface area (r_ρ = .45, p < .01, n=29). For each observer, contrast sensitivity is defined as contrast sensitivity averaged across the four polar angle locations and V1 size is defined as the summed cortical surface area of left and right V1 within 0-8° eccentricity (left hemisphere V1 is illustrated in the inset panel).

When we computed the relation between contrast sensitivity and V1 surface area, we did not normalize V1 surface area by the total cortical surface per observer. It is appropriate to do so if neural density is similar across observers, as in this case, surface area would be a good proxy for neural count. At least in rodents, animals with larger brains have larger neurons, so that the number of neurons is approximately conserved across animals despite differences in brain size (31). Were this also the case for the human brain, it would be appropriate to normalize each observer's V1 surface area by their total cortical surface area. When we normalize by total cortical surface area and then correlate with contrast sensitivity, there remains a positive correlation between the variables (r=.31, p = .05; **Figure S3**).

Quantifying the relation between contrast sensitivity and local V1 surface area measurements along polar angle meridians

Next, we assessed the relation between contrast sensitivity and V1 surface area at a finer granularity. Across observers, we asked whether contrast sensitivity at each meridian correlated with V1 surface area measurements taken from the corresponding wedge-ROI. Each wedge-ROI was ±15° in width, extended from 1° to 8° eccentricity, and was centered along a meridian corresponding to the contrast sensitivity measurements. Spearman's rho was used to assess the relation between contrast sensitivity measurements taken at each of the left and right horizontal, upper, and lower vertical meridians and the surface area of the ±15° wedge-ROI centered on the meridian corresponding meridian. As the data points were not independent, with a data point from each observer per polar angle location, we computed a null distribution by bootstrapping 1000 Spearman's rho correlations and on each iteration we shuffled the assignment of the four contrast sensitivity and four local surface area values across observers. We then calculated the r_ρ value at the 95th percentile ($x_{0.95}$) (32) of this bootstrapped r_ρ distribution. If the reported r_ρ value falls above $x_{0.95}$ then it is greater than 95% of the bootstrapped null distribution values. Histograms of the bootstrapped distributions are available in **Figure S4A.**

Across polar angle locations, contrast sensitivity measurements were positively correlated with the corresponding V1 surface area (r_ρ = .62, $x_{0.95}$ = .56; **Figure 4**). A similar relation between contrast sensitivity and local surface area was found using measurements on the pial (**Figure S5A**) or white matter surface (**Figure S5B**). Thus, local V1 surface area (or, equivalently, cortical magnification) predicted local contrast sensitivity measurements taken from different polar angle locations.

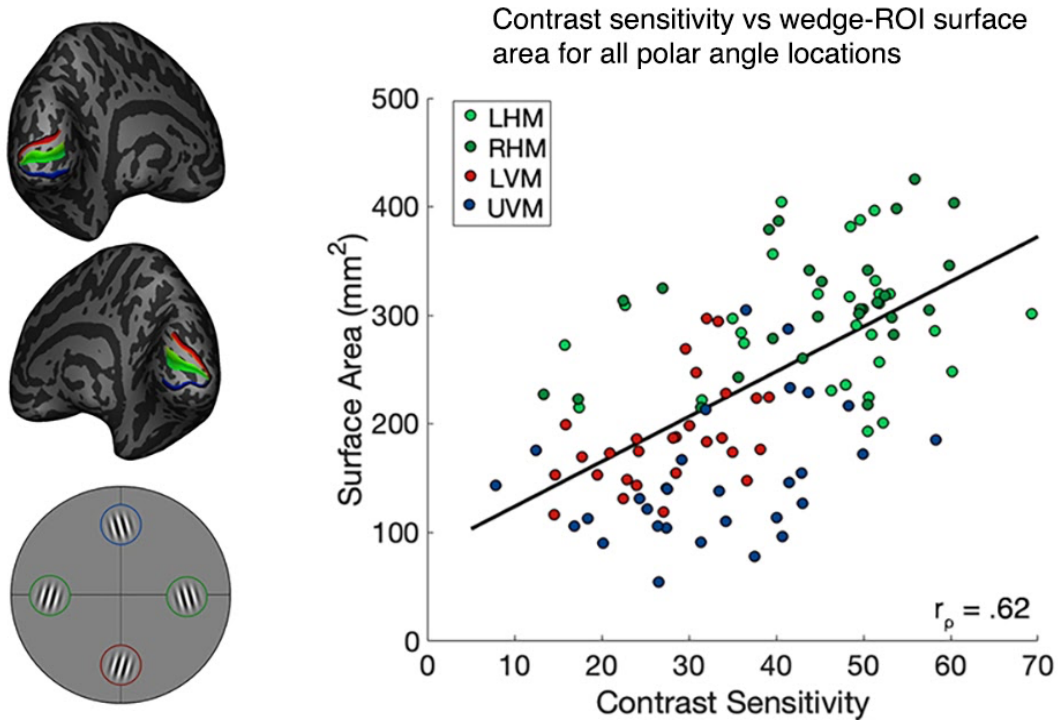

Figure 4. Contrast sensitivity correlates with local V1 surface area (i.e., cortical magnification) measurements taken from the corresponding meridians (n=29). We correlate contrast sensitivity and V1 surface area of ±15° wedges centered on the respective polar angle meridians (r_ρ = .62, $x_{0.95}$ = .56). Data are color-coded to reflect the meridian from which they come from; green data are measurements from the left and right horizontal meridian, red data come from the lower vertical meridian, and blue data come from the upper vertical meridian.

The correlation in **Figure 4** above includes both within- and between-observer variability. We next assessed the separate contributions of within-observer variability (i.e., variability across polar angle locations) and between-observer variability (i.e., variability across individual observers) associated with this correlation. Again, we calculated the null distribution by bootstrapping 1000 Spearman's rho correlations, shuffling the assignment of the contrast sensitivity and local surface area data on each iteration, and calculated the 95th percentile of the bootstrapped r_ρ null distribution. Histograms of the bootstrapped distributions are available in **Figure S4B and C**.

To assess the contribution of within-observer variability (by factoring out between-observer variability), for each observer, we averaged their contrast sensitivity across the four polar angle locations and then subtracted each of the four contrast sensitivity measurements from this averaged value. This was repeated for the local V1 surface area measurements. After factoring out between-observer variability, there was still a positive relation between local contrast sensitivity and local V1 surface area (r_ρ = .78, $x_{0.95}$ = .79; **Figure 5A**). This indicates a robust effect of polar angle. Next, to assess the contribution of between-observer variability (by factoring out within-observer variability), we averaged contrast sensitivity for each of the four meridians across all 29 observers (resulting in one group average value per meridian). We then subtracted each individual observer's contrast sensitivity values from the group-average contrast sensitivity, for

each respective meridian. This was repeated for the local V1 surface area measurements. After accounting for between-observer variability, there was still a positive relation between local contrast sensitivity and local cortical surface area ($r_\rho = .28$, $x_{0.95} = .21$; **Figure 5B**). This indicates a positive, modest effect of individual observer variation in the data.

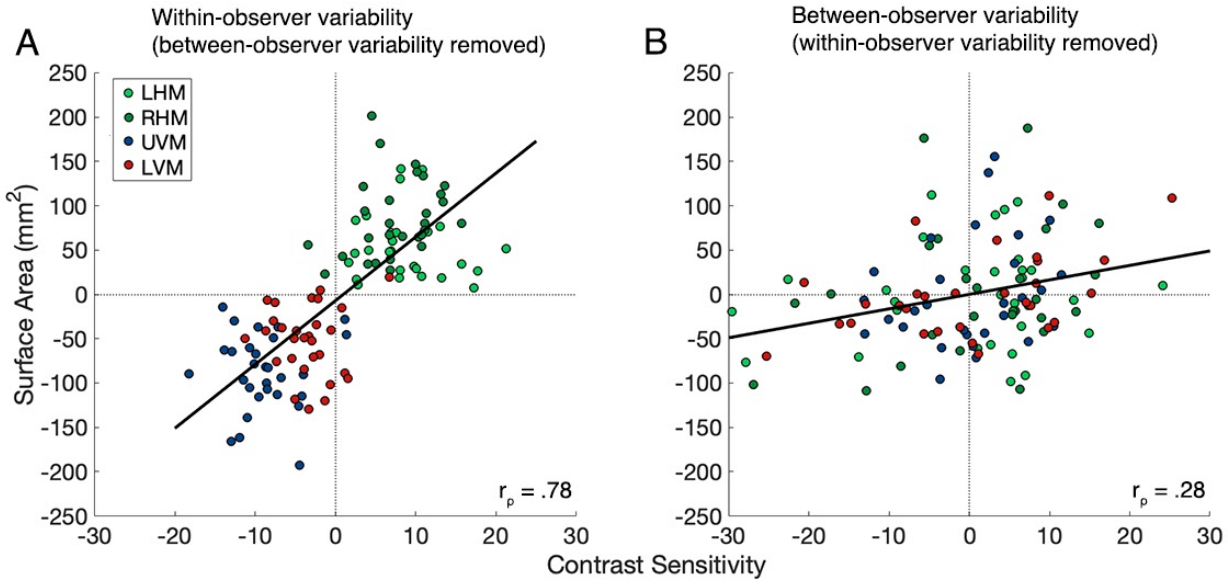

Figure 5. Correlations assessing the contribution of within-observer variability and between-observer variability to the relation between local contrast sensitivity and local V1 surface area. In **(A)** the between-observer variability is removed from the correlation to show the effect of meridian ($r_\rho = .78$, $x_{0.95} = .79$), whereas in **(B)** the within-observer variability is removed from the correlation to show the effect of individual observers ($r_\rho = .28$, $x_{0.95} = .21$).

Quantifying the relation between the strengths of the behavioral and cortical HVA and VMA.

Next, we assessed the relation between the strength of behavioral and cortical HVA and VMA across individual observers. Importantly, HVA and VMA strengths reflect *differences in contrast sensitivity, or V1 surface area*, *between locations*, after dividing out the mean contrast sensitivity, or local V1 surface area, per observer. Therefore, one could have low contrast sensitivity, but a strong HVA.

Spearman's rho was used to assess the relation between the HVA index for contrast sensitivity and local V1 surface area across observers; there was a significant, positive correlation between the two measurements ($r_\rho = .63$, $p < .001$; **Figure 6A**). A similar correlation was found when the wedge-ROIs were used to calculate V1 surface area measurements on the pial (**Figure S6A**) or white matter surfaces (**Figure S6C**). Thus, observers with a stronger asymmetry in contrast sensitivity measurements between the horizontal and the vertical meridian had a stronger asymmetry in surface area between the horizontal and vertical meridian.

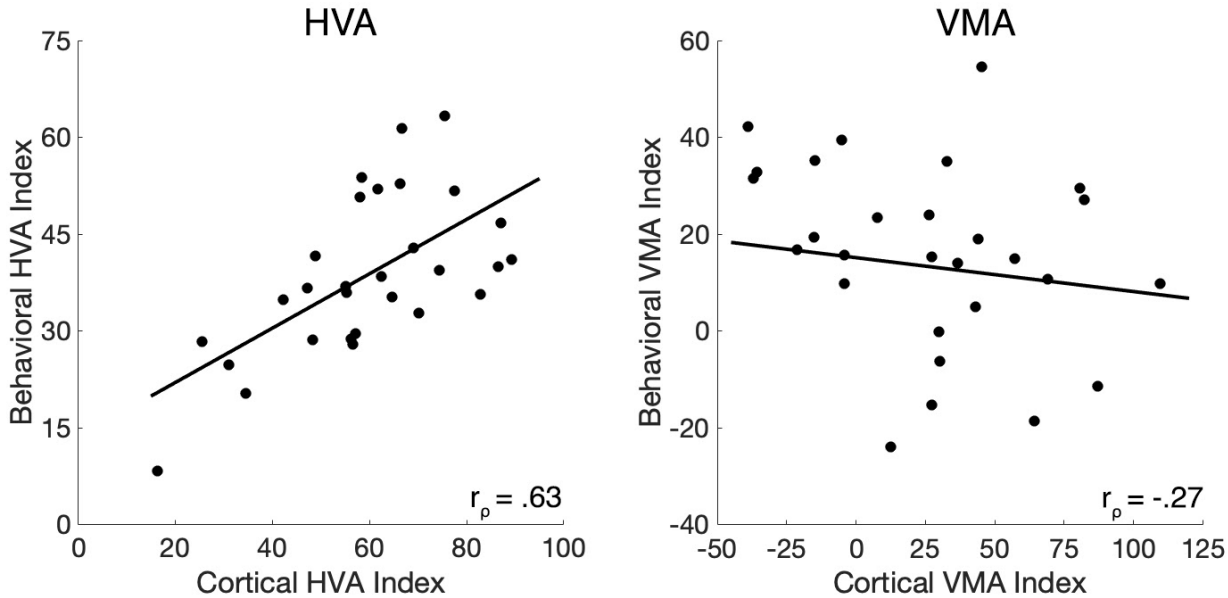

Figure 6. The behavioral and cortical HVA correlate (r_ρ = .63, p < .001) **(B)**, however the cortical and behavioral VMA do not (r_ρ = -.27, p > .1).

Following this, Spearman's rho was used to test the relation between the VMA index for contrast sensitivity and local V1 surface area; however, there was no significant correlation between the two measurements (r_ρ = -.27, p > .1; **Figure 6B**). Thus, the asymmetry for contrast sensitivity between the lower and upper vertical meridian was not associated with the amount of V1 surface area dedicated to the lower and upper vertical meridian. There was also no systematic relation when the local V1 surface area measurements were made on the pial (**Figure S6B**) or white matter surface (**Figure S6D**). In a supplemental analysis, we found no significant correlation between the behavioral HVA and VMA (**Figure S7A**), and only a marginal correlation between the cortical HVA and VMA (**Figure S7B**).

DISCUSSION

We quantified the relation between contrast sensitivity and V1 surface area at a global (i.e., the surface area of V1 itself) and a local (i.e., the local surface area of V1 processing the polar angle meridians) scale across 29 observers. We confirmed group-level polar angle asymmetries in our contrast sensitivity and V1 surface area data. We then quantified individual differences across observers, leading to three major findings. First, contrast sensitivity averaged across the four polar angle locations positively correlated with total V1 surface area. Second, contrast sensitivity measurements taken at the four polar angle locations positively correlated with localized V1 surface area measurements taken from the corresponding polar angle meridian in the visual field. Third, the extent of the HVA for contrast sensitivity was correlated with the extent of the HVA for V1 surface area, whereas the VMA was not.

Group-level reproduction of polar angle asymmetries

The data showed clear group-level polar angle asymmetries for contrast sensitivity and in V1 surface area. Contrast sensitivity was about 50% higher for the horizontal than vertical meridian, and 20% higher for the lower than upper vertical meridian. Likewise, the V1 surface area measurements also showed group-level polar angle asymmetries; V1 surface area was around 60% greater along the horizontal than vertical meridian, and around 25% greater along the lower than upper vertical meridian, consistent with data from our previous study (7), the Human Connectome Dataset (8) and other work (20, 33). Polar angle asymmetries have also been found in the surface areas of non-human primate V1 (6), and in the amplitude of the BOLD response in human V1 (33, 34). The existence of these polar angle asymmetries in multiple, large datasets for both the behavioral and cortical data indicates that they are robust at the group-level.

The present group-level data, and an extended dataset (n=54; an additional 25 subjects with MRI data only; see Supplemental Information), showed a small bias towards more V1 surface area dedicated to the right than left horizontal meridian. It might be that a left-right horizontal asymmetry relates to visual tasks in which an advantage along the right horizontal meridian exists, such as crowding (35–37) and letter recognition (38, 39). A larger left than right hemisphere V1 has been previously reported ((4), but see (2, 20)). However, none of these studies examined the surface area of the horizontal meridian specifically.

Variation in the size of V1 surface area across observers

The surface area of V1 varied substantially among observers, whereas within observers, the surface area of V1 in the left and right hemispheres was relatively consistent, in line with previous studies (1, 2, 4, 6, 40). V1 size is only weakly correlated with overall cortical surface area, which is less variable in size, as shown here and in prior reports (2, 41). Neither does V1 size differ between males and females after normalization to total cortical surface area, again shown here and previously (2). V1 size correlates with the size of the lateral geniculate nucleus and the optic tract, indicating that components of the visual system, which are important for visual perception, develop interdependently (1). This lends credence to the possibility that the size of V1 is important for perceptual tasks.

Greater contrast sensitivity is a perceptual consequence of greater V1 surface area

Here, we have shown that contrast sensitivity measurements derived from an orientation discrimination task positively correlate with V1 surface area; observers with greater contrast sensitivity tend to have a larger V1, and those with lower contrast sensitivity tend to have a smaller V1. This relation holds irrespective of the cortical depth used to compute surface area (gray/pial boundary, gray/white boundary, or half-way between them). V1 surface area has been shown to correlate with a few measurements of visual performance, such as perceptual acuity thresholds (42, 43), orientation discrimination thresholds (but not contrast discrimination thresholds) (44), and measurements of subjective object size (41). Nonetheless, performance on

most visual tasks have not been compared to V1 size, and there is not yet a computational account that would enable one to predict to what extent, if any, performance on different tasks would be affected by V1 size.

We focused on the relation between performance on one visual measure – contrast sensitivity – and the size of the one cortical map – V1. Although V1 size has been linked to a few perceptual measures (41–44), it is likely that there will be other measures for which performance is better explained by the size of other visual areas. Such an outcome is possible because the sizes of different maps are at least partially independent (2, 4). For example, an observer might have a large V1 and high contrast sensitivity, but a small hV4 and poor performance on visual crowding tasks (45).

An open question is whether, and how, the variation in the size of V1 relates to neural circuitry. Smaller V1s have a full, but relatively compressed, representation of the visual field. Does this compression represent fewer overall neurons, or is neural count similar across individuals and instead this compression represents increased neural density? The fact that performance on at least some tasks correlates with V1 surface area (41–44) implies that a smaller V1 likely has fewer overall neurons, but the histological measures do not yet exist. Differences in V1 neural counts among individuals and across polar angle, raise the question of how the neural code varies across individuals and visual field location. One interesting observation is that the size of V1 is inversely correlated with the size of its pRFs, suggesting that a larger V1 enables finer sampling of visual space (46).

Local contrast sensitivity is related to local V1 cortical magnification around the visual field

Virsu and Rovamo (1979; (27)) hypothesized that the mechanism underlying contrast sensitivity is a central integrator that pools the activity of V1 neurons; contrast sensitivity should increase in proportion to local cortical surface area (i.e., cortical magnification) and thus the number of neurons activated by a stimulus. This hypothesis was derived from group-level behavioral measurements taken as a function of eccentricity. We have tested whether this hypothesis holds for individual, localized V1 surface area measurements taken as a function of polar angle, as well as for individual measurements of the entire area of V1. We found that observers with more local cortical surface area dedicated to processing some polar angle location had greater contrast sensitivity at the corresponding location, and that individuals with larger V1 had overall higher contrast sensitivity. Therefore, our data support the hypothesis that contrast sensitivity varies as a function of the number of stimulated visual neurons.

Prior studies have related the surface area of entire visual maps to perceptual measurements. Advances in computational neuroimaging provide the tools to precisely delineate visual maps and assess their internal layout, thereby allowing one to assess the relation between cortical anatomy and performance as a function of location in the visual field. The only prior study relating individual differences in cortical magnification to perceptual outcomes reported a positive

correlation between V1 cortical magnification and visual acuity measured as a function of eccentricity (3).

Performance field asymmetries

Perceptual polar angle asymmetries ('*performance fields*') have been established across a broad range of visual tasks. The HVA and VMA are found in tasks involving contrast sensitivity (13, 14, 16, 47–53), perceived contrast (54), spatial resolution (15, 55, 56), temporal information accrual (57), illusory motion perception (17) and visual short term memory (58). Further, these polar angle asymmetries are pervasive across a range of conditions; they exist across luminance levels (13), binocular and monocular stimulation (13, 15), different stimulus orientations (13, 48, 53), eccentricities and spatial frequencies (13, 14, 16, 48) as well as covert attentional conditions (13, 14, 18, 19).

We found no relation between the behavioral HVA and VMA, consistent with previous reports (15, 16), and only a weak, non-significant relation between the cortical HVA and VMA. These results suggest that the HVA and VMA are independent from each other at the level of perception *and* at the level of the cortex. It is likely that these two behavioral asymmetries develop with age independently (59) and may have separate neural substrates. It has been found that cortical magnification changes as a function of eccentricity and polar angle, for the horizontal vs vertical meridian, in a similar fashion for children and adults (60); however, the cortical HVA and VMA have not been assessed for children. Furthermore, the HVA, but not VMA, exists in photoreceptor cone density (61, 62), whereas both the HVA and VMA exist in retinal midget ganglion cell density (63, 64).

Individual differences in perceptual polar angle asymmetries are rooted in individual variation in cortical anatomy

Here, we have shown that the HVA for contrast sensitivity can be predicted from the cortical HVA in individual observers. Thus, the perceptual asymmetry between the horizontal and vertical meridian for contrast sensitivity is strongly reflected by the relative distribution of V1 surface area between the horizontal and vertical meridian. The findings that the behavioral and cortical HVA can be linked across individual observers, and is stronger in the visual cortex than the retina (8, 65), suggest that this perceptual asymmetry can be predominantly explained by the asymmetric distribution of cortical surface, and thus neurons, in V1.

Although we found group-level VMA measurements for contrast sensitivity and surface area, and prior work shows that group-level VMA measurements for spatial acuity thresholds and V1 surface area correlate (8), we did not find a relation at the level of individual differences. Why might this be? One possibility is statistical power. The VMA is computed using half the amount of data as the HVA (i.e., the upper vs lower vertical meridian, rather than the left and right horizontal combined vs the upper and lower vertical combined), and the strength of the asymmetry is about half the size. Another possibility is measurement constraints. Unlike the

horizontal meridian, which extends through the approximate middle of the calcarine sulcus, the vertical meridian falls along the border of V1 and V2. fMRI measurements are more difficult near areal boundaries, thereby impacting the precision of vertical meridian measurements at the individual level. Alternatively, individual differences in the behavioral VMA might be explained, at least in part, by factors other than the total computational resources (e.g., surface area) afforded by V1. For example, individual differences in the VMA might be dependent upon the tuning properties of neurons within V1, or by the efficiency of how the V1 outputs are readout by neurons in downstream visual maps.

Conclusion

We have quantified the relation between contrast sensitivity and V1 surface area, measured as a function of polar angle, across the same observers. Our data showed that: First, observers with greater contrast sensitivity tended to have a larger V1, and vice versa. Second, local contrast sensitivity can be predicted by local V1 surface area using measurements taken from the polar angle meridians. Third, a stronger horizontal-vertical asymmetry in contrast sensitivity corresponds to a stronger horizontal-vertical asymmetry in the distribution of local V1 surface area. Overall, these findings confirm that individual differences in contrast sensitivity can be linked to individual differences in V1 surface area at a global and local scale and reveal that perceptual polar angle asymmetries are rooted in the cortical anatomy of V1. More broadly, our findings show that there is a tight link between visual perception and the idiosyncratic cortical organization of V1 of neurotypical observers.

METHODS

Observers

29 observers (18 females, 11 males, mean age = 29.9 years, including two authors: MMH and JW) were recruited from New York University. All observers had normal or corrected-to-normal vision and completed two experimental sessions: a 1-hour psychophysics session and a 1-1.5-hour fMRI scanning session. All observers provided written informed consent. The experiment was conducted in accordance with the Declaration of Helsinki and was approved by the New York University ethics committee on activities involving human observers.

Psychophysics experiment: Measuring contrast sensitivity around the visual field

The methods used here are identical to the methods used to acquire the behavioral data in our previous study (16). The behavioral data for 9 of the 29 observers reported here are the same as we reported in the baseline condition of that study.

Apparatus and set up

Observers completed the psychophysics session in a darkened, sound attenuated room. Stimuli were presented on a 21-inch ViewSonic G220fb CRT monitor (1280 x 960 resolution, 100 Hz) and were generated using an Apple iMac (3.2 GHz, Intel Core i3) in MATLAB 2017a (Mathworks, Natick, MA). The CRT monitor was gamma corrected with a ColorCal MKII colorimeter (Cambridge Research Systems, Rochester, Kent, UK) to ensure a linear relation between the frame buffer values and screen luminance. Observers viewed the monitor display binocularly with their head stabilized in a chin rest that was 57cm from the monitor. An EyeLink 1000 eye tracker (SR Research, Ottawa, Ontario, Canada) with a sampling rate of 1000 Hz was used to measure fixation throughout the experiment.

Stimuli

The psychophysical stimulus was a Gabor patch (a sinusoidal grating embedded in a Gaussian envelope) presented on a uniform grey background. The Gabor was presented at four polar angle locations (0° on the right horizontal meridian, 90° on the upper vertical meridian, 180° on the left horizontal meridian, and 270° on the lower vertical meridian) at 4.5° eccentricity from the center of the display. The Gabor patch had a spatial frequency of 4 cycles per degree (cpd) and covered 3° of visual angle (σ = 0.43°). The Gabor patch was oriented ±15° from vertical; the orientation of the stimulus changed trial-by-trial. The contrast of the stimulus also changed trial-by-trial, based on the titration procedure.

In the center of the display was a black fixation across (0.5°). A set of four stimulus placeholders consisting of four small black squares (each 4 pixels in size) were placed just above, below, to the left, and to the right of the four locations that the Gabor patch could appear. These placeholders were included to remove spatial uncertainty about the locations the Gabor patch could appear. The placeholders remained on the screen throughout the entire experiment.

Experimental Design

Contrast thresholds were measured at each of the four locations. To do so, observers completed a two-alternative forced choice (2AFC) orientation discrimination task in which the Gabor patch contrast was titrated using four randomly interleaved 3-down 1-up staircases via parameter estimation by sequential testing (PEST; (66). The staircases converged at 79.4% performance accuracy threshold. The staircases were interleaved across trials, and one staircase was dedicated to each of the four visual field locations. A schematic and description of a single trial is presented in **Figure 7**.

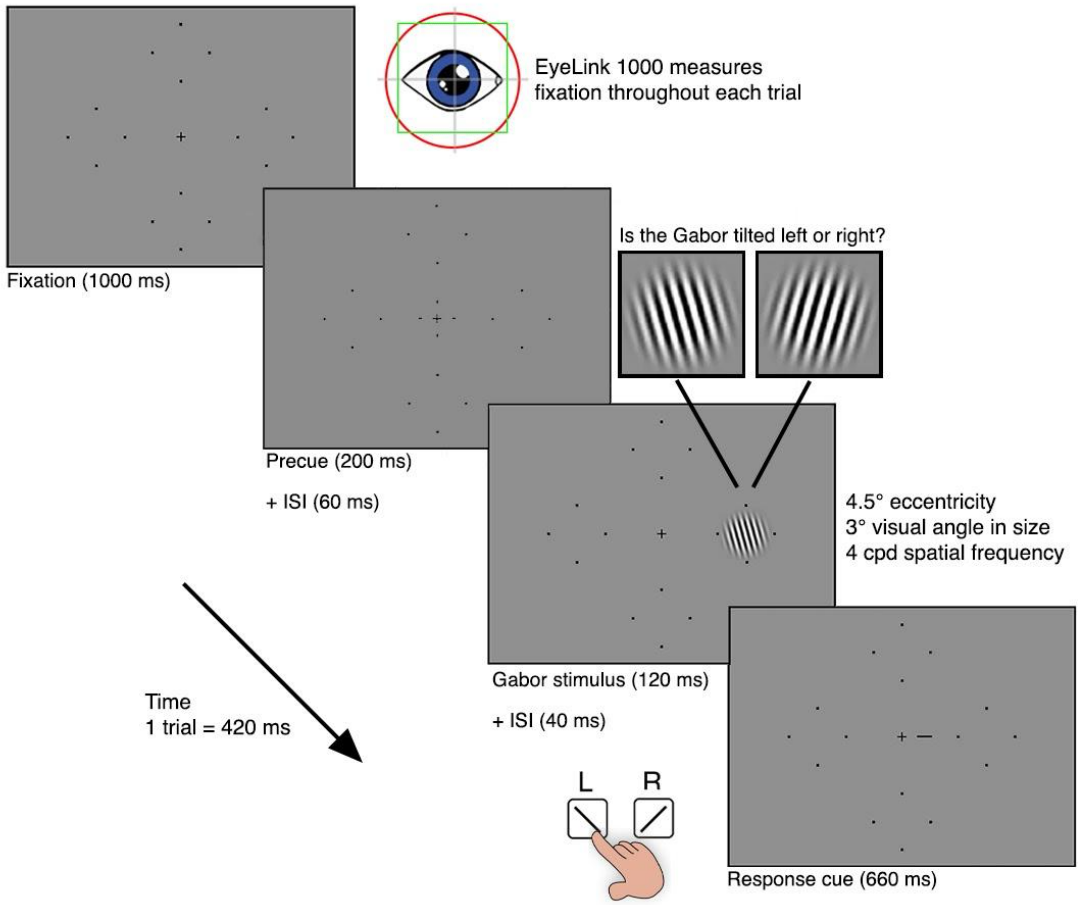

Figure 7. Orientation discrimination task to measure contrast sensitivity at the four polar angle locations. Each trial begins with 1000 ms of fixation measured via an EyeLink eye tracker. This is followed by a 200 ms pre-stimulus cue to indicate the onset of the trial and a 60 ms inter-stimulus-interval (ISI). A Gabor patch is then presented at one of the four possible polar angle locations for 120 ms. The Gabor patch is tilted either left or right (±15°) from vertical. The offset of the Gabor patch is followed by a 40 ms ISI. A response cue (a small line indicating the location at which the Gabor patch appeared) is then presented on the screen for 660 ms. This response cue was used to eliminate uncertainty regarding the target location at very low contrasts. A brief auditory tone signaled that the observer had 5000 ms to respond, via the keyboard, as to whether the Gabor patch was tilted left or right from vertical. Auditory feedback was provided in the form of a tone to inform the observer as to whether their response was correct or incorrect. This was followed by a 1000 ms ITI before the beginning of the next trial.

In accordance with PEST rules, the Michelson contrast of the Gabor patch was titrated across trials (67). Any trials in which the observer broke fixation (eye movements > 1.5° from fixation) were aborted and added to the end of the experimental block. Observers were allowed to break fixation and blink during the response period and the ITI.

Five blocks, each consisting of 200 trials (50 trials per location), were acquired for each observer. During each block, observers were given a 20 second break after 100 trials before completing the remaining trials. Prior to completing the experiment, observers completed 1 block of 24 practice trials in which the Gabor stimuli was set to 100% contrast to ensure they were comfortable with the orientation discrimination task, eyetracking, and stimulus timing.

The 79.4% performance accuracy contrast thresholds at each of the four locations were averaged across the five independent blocks. Contrast sensitivity values were calculated as the reciprocal of these thresholds.

fMRI Experiment: Retinotopic mapping and defining wedge-ROIs on the visual field meridians

Each observer completed a 1 - 1.5-hour scan session in which they participated in a retinotopic mapping experiment to measure population receptive field (pRF) polar angle and eccentricity estimates across visual cortex. These estimates were then used to delineate each observer's V1 map and to calculate the surface area of ±15° wedge-ROIs centered on the same angular locations as the contrast sensitivity measurements.

The pRF stimulus, MRI and fMRI acquisition parameters, MRI and fMRI preprocessing, and the implementation of the pRF model are identical to those in our prior work (7). The retinotopic data for 17 of the 29 observers reported here are the same as reported in that study.

fMRI stimulus display

Observers viewed a population receptive field (pRF) stimulus from inside the MRI scanner bore using a ProPixx DLP LED Projector (VPixx Technologies Inc., Saint-Bruno-de-Montarville, QC, Canada). The pRF stimulus was projected onto an acrylic back-projection screen (60cm x 36.2cm) within the scanner bore. The projected image had a resolution of 1920 x 1080 and a refresh rate of 60 Hz. The display was calibrated using a linearized lookup table and the display luminance was 500 cd/m^2. Observers viewed the screen at a distance of 83.5 cm (from eyes to the screen) using an angled mirror that was mounted on the head coil.

pRF stimulus

Retinotopic maps were measured using pRF mapping (68). The pRF stimulus was generated on an iMac computer using MATLAB 2017a and was projected onto the fMRI stimulus display in the scanner bore using the Psychophysics Toolbox v3 (69) and custom *vistadisp* software (https://github.com/WinawerLab/vistadisp).

The pRF stimulus consisted of image patterns presented within a bar aperture that swept across the screen for the duration of each scan. The image patterns consisted of colorful objects, faces, and scenes at multiple scales that were superimposed on an achromatic pink noise (1/f) background (70, 71). The image pattern was windowed within a circular aperture that had a radius of 12.4°. The image pattern was revealed through a bar aperture (3.1° wide, or 1/8th of the full stimulus extent) that swept across the screen in 24 equal steps (once per second). Each step was synchronized to the MR image acquisition (TR 1 second). There were 8 sweeps in total. Each sweep began at the edge of the circular aperture. Horizontal and vertical sweeps covered the entire diameter of the circular aperture. Diagonal sweeps only traversed half of the circular

aperture; the second half of these sweeps were replaced with a blank gray screen. Each directional sweep lasted 24 s. The full stimulus run lasted 192 s. The stimulus image updated 3 times per second without intermediate blanks (3 Hz).

The bar aperture was superimposed on a polar fixation grid placed upon a uniform gray background, with a red or green dot at the center (3 pixels, or 0.07°). Observers were instructed to maintain fixation throughout the entire scan and completed a fixation task in which they were required to respond, using a button box, when the fixation dot changed from green to red, or vice versa.

The full stimulus sequence was completed once per functional scan. The identical aperture sequence was shown in each of the scans.

Anatomical and functional data acquisition

Anatomical and functional data were acquired on a 3T Siemens MAGNETOM Prisma MRI scanner (Siemens Medical Solutions, Erlangen, Germany) using a Siemens 64-channel head coil. A T1-weighted (T1w) MPRAGE anatomical image was acquired for each observer (TR, 2400 ms; TE, 2.4 ms; voxel size, 0.8mm^3 isotropic; flip angle, 8°). This anatomical image was auto-aligned to a template to ensure a similar slice prescription for all observers. Between 4 and 12 (9x had 12 scans, 2x had 11 scans, 2x had 10 scans, 5x had 8 scans, 1x had 7 scans, 8x had 6 scans, 1x had 5 scans, and 1x had 4 scans) functional echo-planar images (EPIs) were acquired for each observer using a T2*-weighted multiband EPI sequence (TR, 1000 ms; TE, 37 ms; voxel size, 2mm^3; flip angle, 68°; multiband acceleration factor, 6; phase-encoding, posterior-anterior) (72, 73). Two distortion maps were also acquired to correct susceptibility distortions in the functional images: one spin-echo image with anterior-posterior (AP) phase encoding and one with posterior-anterior (PA) phase encoding.

Preprocessing of structural data

fMRIPrep v.20.0.1 (74, 75) was used to preprocess anatomical and functional data. For each observer, the T1w anatomical image was corrected for intensity inhomogeneity and then skull stripped. The anatomical image was automatically segmented into cerebrospinal fluid, cortical white-matter, and cortical gray-matter using *fast (76)*. Cortical surfaces were reconstructed using Freesurfer's *recon-all* (77) and an estimated brain mask was refined using a custom variation of the method.

Preprocessing of functional data

The following preprocessing was performed on each observer's functional data. First, a reference volume (and a skull stripped version) was generated using custom methodology of *fMRIPrep*. The two spin echo images with opposing phase-encoding directions (i.e., AP and PA distortion maps) were used to estimate a B0-nonuniformity map. The estimated distortion of the

B0-nonuniformity map was then used to generate a corrected functional reference image. This corrected functional reference was co-registered to the anatomical image using six degrees of freedom.

Next, head-motion parameters with respect to the functional reference were estimated before any spatiotemporal filtering. Each functional image was slice-time corrected with all slices realigned to the middle of each TR. The slice-time corrected functional data were then resampled to the T1w anatomical space via a one-shot interpolation consisting of all the pertinent transformations (i.e., head-motion transform matrices, susceptibility distortion correction). These preprocessed time-series data were then resampled to the *fsnative* surface by averaging across the cortical ribbon.

Implementing the pRF model to produce retinotopic maps

The pRF model was implemented on the *fsnative* surface of each individual observer. For each *fsnative* vertex, the time-series data across each functional scan were averaged together to generate an average time-series. These average time-series were then transformed to BOLD percent signal change (i.e., % change at each TR from the mean signal across all TRs). The pRF model was fit to the BOLD signal change.

The pRF model was implemented using *vistasoft* (https://vistalab.stanford.edu/software/, Vista Lab, Stanford University) and customized code to run the model on the cortical surface. A pRF was modelled as a circular 2D-Gaussian that was parameterized by values for x, y, and σ. The x and y parameters specify the center position of the 2D-Gaussian in the visual field, whereas the σ parameter, the standard deviation of the 2D-Gaussian, specifies the size of the receptive field. The 2D-Gaussian was multiplied pointwise by the stimulus contrast aperture and was then convolved with a hemodynamic response function (HRF) to predict the BOLD percent signal change. We parameterized the HRF by 5 values, describing a difference of two gamma functions, as used previously (46, 68, 78, 79).

The pRF model was implemented using a coarse-to-fine approach to find the optimal x, y, and σ for each vertex by minimizing the residual sum of squares between the predicted time-series and BOLD signal (68). The x and y values were then used to calculate vertex-wise eccentricity and polar angle coordinates, reflecting the pRF center position in the visual field.

Defining V1

V1 was defined as a region-of-interest (ROI) by hand using Neuropythy v0.11.9 (https://github.com/noahbenson/neuropythy; (80). We defined V1 from 0°-8° eccentricity with the V1/V2 dorsal border falling through the center of the lower vertical meridian, and the V1/V2 ventral border falling through the center of the upper vertical meridian.

Defining wedge-ROIs

To calculate local measurements of V1 surface area along the polar angle meridians, we defined ±15° wedge-ROIs that were centered along each of the four polar angle meridians in the visual field. We then measured the amount of V1 surface area within these wedge-ROIs (7). As the wedge-ROIs at each meridian are always defined to encapsulate ±15° of visual space, any differences in the amount of localized V1 surface area calculated using these wedge-ROIs can be interpreted as a measurement of cortical magnification.

In brief, we defined ±15° wedge-ROIs that were centered on the left and right horizontal meridians, and the upper and lower vertical meridians in the visual field. Each wedge-ROI extended from 1°-8° eccentricity. Unlike the 0°-8° limit we used for mapping V1 size, we excluded the central 1° from the wedge-ROIs because the polar angle representations are hard to distinguish in the foveal representation (4, 81). Each wedge-ROI was used as a mask and was overlaid on *cortical surface area maps*; these maps specify the cortical surface area (in mm^2) of each vertex on the *fsnative* midgray cortical surface. In supplemental analyses, we overlaid the wedge-ROIs on the pial and white matter cortical surfaces; this is because the surface area changes as a function of cortical depth. The surface area of gyri at the pial surface and the sulci at the white matter surface tend to be large, whereas the reverse (sulci at the pial surface and gyri at the white matter surface) are relatively smaller. The cortical surface area encapsulated by each wedge-ROI mask was calculated by summing the surface area of V1 vertices falling within that mask. This calculation outputs the V1 surface area dedicated to processing each wedge-ROI.

To calculate the surface area dedicated to processing the full horizontal meridian, the surface area of the left and right horizontal wedge-ROIs was summed together. To calculate the surface area dedicated to processing of the upper vertical meridian, the surface area of the wedge-ROIs extending the left and right sides of the upper vertical meridian (thus right and left hemispheres of V1, respectively) were summed together. Likewise, to calculate the surface area dedicated to processing the lower vertical meridian, the wedge-ROIs extending the left and right sides of the lower vertical meridian (again, right and left hemispheres of V1, respectively) were summed together to calculate the surface area dedicated to processing the lower vertical meridian. These upper and lower vertical meridian wedge-ROIs were combined to calculate the surface area dedicated to processing the full vertical meridian.

Summary to relate psychophysical and fMRI analyses

Figure 8 summarizes how the contrast sensitivity measurements relate to the wedge-ROIs measurements of local V1 surface area. Contrast sensitivity was measured at four polar angle locations: the left and right horizontal, upper vertical, and lower vertical meridians (**Figure 8A**). Contrast sensitivity measurements were made using Gabor patches that are 3° of visual angle in size and were placed at 4.5° eccentricity from fixation. Next, we calculated the pooled surface area of V1 vertices falling within ±15° wedge-ROIs that were centered along the horizontal (green

mask), upper vertical (blue mask) and lower vertical (red mask) meridians (**Figure 8B**, left hemisphere V1/right visual hemifield). These measurements are calculated for the left and right hemisphere (thus the wedge-ROIs were centered on each meridian and extend 15° either side). As the upper and lower vertical meridian is split across hemispheres, the ±15° wedge-ROIs for these meridians were formed by combining the V1 surface area of the 15° wedges that encapsulated data from the left and right portions of V1.

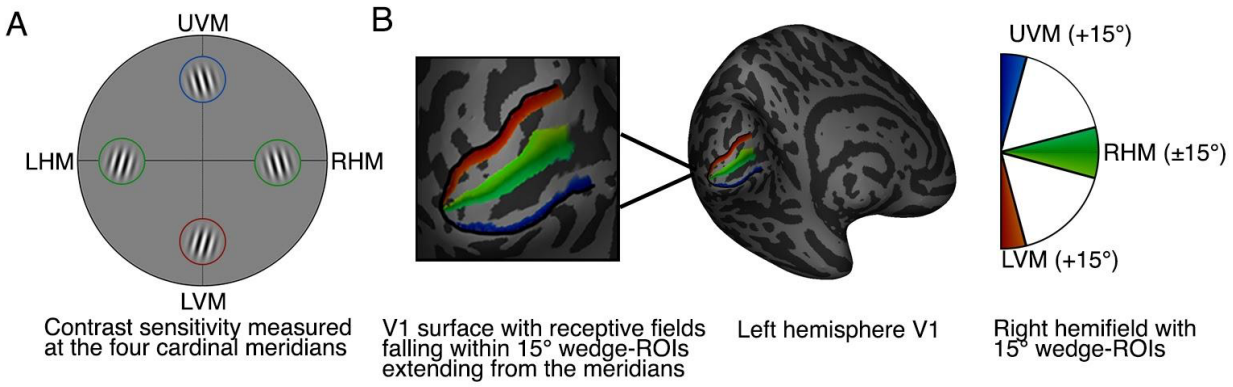

Figure 8. (A) Contrast sensitivity is measured at the four polar angle meridians using an orientation discrimination task. **(B)** 15° wedge-ROIs are defined in the visual field and extend from each of the four polar angle meridians that match the angular location of the contrast sensitivity measurements. The V1 surface area dedicated to processing the regions of visual space within the wedge-ROI mask is calculated. The surface area of each wedge-ROI is summed across the left and right hemispheres to form a ±15° wedge centered on each meridian.

Therefore, we calculated measures of cortical magnification along the polar angle meridians that matched the angular location of contrast sensitivity measurements. Note that we do not intend for our cortical magnification measurements to be an exact measurement of the amount of V1 surface area dedicated to processing the Gabor stimulus itself (i.e., a 3° x 3° patch at 4.5° of eccentricity in V1 at each polar angle meridian). Measurements of cortical magnification are noisy, and the more data included in the calculation of the surface area of the wedge-ROI, the more accurate the output value. We chose to measure the surface area of wedge-ROIs ±15° in angle when the Gabor patches in the visual field extend ±1.5° either side of each polar angle meridian. This is because there is a tradeoff in the width of the wedge-ROI and the accuracy of cortical magnification measurements (especially along the vertical meridian where data is comparatively sparse when compared to the horizontal meridian) (7).

ACKNOWLEDGEMENTS

This research was funded by the US NIH National Eye Institute R01-EY027401 to MC and JW. We thank Michael Jigo, Eline Kupers and Ekin Tünçok for their feedback on the manuscript.

REFERENCES

1. T. J. Andrews, S. D. Halpern, D. Purves, Correlated size variations in human visual cortex, lateral geniculate nucleus, and optic tract. *Journal of Neuroscience* **17** (1997).

2. N. C. Benson, J. M. Yoon, D. Forenzo, S. A. Engel, K. N. Kay, J. Winawer, Variability of the surface area of the V1, V2, and V3 maps in a large sample of human observers. *bioRxiv* (2021).

3. R. O. Duncan, G. M. Boynton, Cortical magnification within human primary visual cortex correlates with acuity thresholds. *Neuron* **38**, 659–671 (2003).

4. R. F. Dougherty, V. M. Koch, A. A. Brewer, B. Fischer, J. Modersitzki, B. A. Wandell, Visual field representations and locations of visual areas v1/2/3 in human visual cortex. *J. Vis.* **3**, 586–598 (2003).

5. J. C. Horton, The representation of the visual field in human striate cortex. *Arch. Ophthal.* (1991) https:/doi.org/10.1001/archopht.1991.01080060080030.

6. D. C. Van Essen, W. T. Newsome, J. H. R. Maunsell, The visual field representation in striate cortex of the macaque monkey: Asymmetries, anisotropies, and individual variability. *Vision Res.* (1984) https:/doi.org/10.1016/0042-6989(84)90041-5.

7. M. M. Himmelberg, J. W. Kurzawski, N. C. Benson, D. G. Pelli, M. Carrasco, J. Winawer, Cross-dataset reproducibility of human retinotopic maps. *Neuroimage* **244**, 118609 (2021).

8. N. C. Benson, E. R. Kupers, A. Barbot, M. Carrasco, J. Winawer, Cortical magnification in human visual cortex parallels task performance around the visual field. *Elife* **10** (2021).

9. P. M. Daniel, D. Whitteridge, The representation of the visual field on the cerebral cortex in monkeys. *J. Physiol.* **159**, 203–221 (1961).

10. S. A. Engel, *et al.*, fMRI of human visual cortex. *Nature* **369**, 525 (1994).

11. T. Inouye, *Die Sehstorungen bei Schussverletzungen der Kortikalen Sehsphare: Nach Beobachtungen an Verwundeten der letszten japanischen Kriege* (Engelmann, 1909).

12. G. Holmes, Disturbances of vision by cerebral lesions. *Br. Med. J.* **2**, 193–199 (1919).

13. M. Carrasco, C. P. Talgar, E. L. Cameron, Characterizing visual performance fields: effects of transient covert attention, spatial frequency, eccentricity, task and set size. *Spat. Vis.* **15**, 61–75 (2001).

14. E. L. Cameron, J. C. Tai, M. Carrasco, Covert attention affects the psychometric function of contrast sensitivity. *Vision Res.* **42**, 949–967 (2002).

15. A. Barbot, S. Xue, M. Carrasco, Asymmetries in visual acuity around the visual field. *J. Vis.* **21**, 2 (2021).

16. M. M. Himmelberg, J. Winawer, M. Carrasco, Stimulus-dependent contrast sensitivity asymmetries around the visual field. *J. Vis.* **20**, 18 (2020).

17. S. Fuller, M. Carrasco, Perceptual consequences of visual performance fields: The case of the line motion illusion. *J. Vis.* **9**, 1–17 (2009).

18. N. M. Hanning, M. M. Himmelberg, M. Carrasco, Presaccadic attention enhances contrast sensitivity, but not at the upper vertical meridian. *bioRxiv* (2021) https:/doi.org/10.1101/2021.10.01.461760.

19. S. Purokayastha, M. Roberts, M. Carrasco, Voluntary attention improves performance similarly around the visual field. *Atten. Percept. Psychophys.* (2021) https:/doi.org/10.3758/s13414-021-02316-y.

20. M. F. Silva, J. W. Brascamp, S. Ferreira, M. Castelo-Branco, S. O. Dumoulin, B. M. Harvey, Radial asymmetries in population receptive field size and cortical magnification factor in early visual cortex. *Neuroimage* **167**, 41–52 (2018).

21. D. G. Albrecht, D. B. Hamilton, Striate cortex of monkey and cat: contrast response function. *J. Neurophysiol.* **48**, 217–237 (1982).

22. G. M. Boynton, J. B. Demb, G. H. Glover, D. J. Heeger, Neuronal basis of contrast discrimination. *Vision Res.* **39**, 257–269 (1999).

23. R. L. DeValois, K. K. DeValois, *Spatial Vision* (Oxford University Press, 1991) https:/doi.org/10.1093/acprof:oso/9780195066579.001.0001.

24. D. G. Albrecht, W. S. Geisler, R. A. Frazor, A. M. Crane, Visual cortex neurons of monkeys and cats: temporal dynamics of the contrast response function. *Journal of Neurophysiology* **88**, 888–913 (2002).

25. I. Marquardt, M. Schneider, O. F. Gulban, D. Ivanov, K. Uludağ, Cortical depth profiles of luminance contrast responses in human V1 and V2 using 7 T fMRI. *Hum. Brain Mapp.* **39**, 2812–2827 (2018).

26. G. Sclar, P. Lennie, D. D. DePriest, Contrast adaptation in striate cortex of macaque. *Vision Res.* **29**, 747–755 (1989).

27. V. Virsu, J. Rovamo, Visual resolution, contrast sensitivity, and the cortical magnification factor. *Exp. Brain Res.* **37**, 475–494 (1979).

28. A. J. Rockel, R. W. Hiorns, T. P. Powell, The basic uniformity in structure of the neocortex. *Brain* **103**, 221–244 (1980).

29. D. H. Hubel, T. N. Wiesel, Ferrier lecture. Functional architecture of macaque monkey visual cortex. *Proc. R. Soc. Lond. B Biol. Sci.* **198**, 1–59 (1977).

30. J. C. Caruso, N. Cliff, Empirical Size, Coverage, and Power of Confidence Intervals for Spearman's Rho. *Educ. Psychol. Meas.* **57**, 637–654 (1997).

31. S. Herculano-Houzel, D. J. Messeder, K. Fonseca-Azevedo, N. A. Pantoja, When larger brains do not have more neurons: increased numbers of cells are compensated by decreased average cell size across mouse individuals. *Front. Neuroanat.* **9**, 64 (2015).

32. P. H. Kvam, B. Vidakovic, *Nonparametric Statistics with Applications to Science and Engineering* (John Wiley & Sons, 2007).

33. C. O'Connell, L. C. Ho, M. C. Murphy, I. P. Conner, G. Willstein, R. Cham, K. C. Chan, Structural and functional correlates of visual field asymmetry in the human brain by diffusion kurtosis MRI and functional MRI. *Neuroreport* **27**, 1225 (2016).

34. T. Liu, D. J. Heeger, M. Carrasco, Neural correlates of the visual vertical meridian asymmetry. *J. Vis.* **6**, 1294–1306 (2006).

35. J. W. Kurzawski, A. Burchell, D. Thapa, N. J. Majaj, J. Winawer, D. G. Pelli, An enhanced Bouma model fits a hundred people's visual crowding. *bioRxiv* (2021).

36. A. White, K. Tang, J. Yeatman, The field of view for word recognition: crowding and hemifield asymmetries. *J. Vis.* **20**, 911–911 (2020).

37. J. A. Greenwood, M. Szinte, B. Sayim, P. Cavanagh, Variations in crowding, saccadic precision, and spatial localization reveal the shared topology of spatial vision. *Proc. Natl. Acad. Sci. U. S. A.* **114** (2017).

38. M. Mishkin, D. G. Gorgays, Word recognition as a function of retinal locus. *J. Exp. Psychol.* **43**, 43–48 (1952).

39. N. Worrall, P. Coles, Visual field differences in recognizing letters. *Percept. Psychophys.* **20**, 21–24 (1976).

40. S. S. Stensaas, D. K. Eddington, W. H. Dobelle, The topography and variability of the primary visual cortex in man. *J. Neurosurg.* **40**, 747–755 (1974).

41. D. S. Schwarzkopf, C. Song, G. Rees, The surface area of human V1 predicts the subjective experience of object size. *Nat. Neurosci.* **14**, 28–30 (2011).

42. C. Song, D. S. Schwarzkopf, R. Kanai, G. Rees, Neural population tuning links visual cortical anatomy to human visual perception. *Neuron* **85**, 641–656 (2015).

43. M. F. Silva, B. M. Harvey, L. Jorge, N. Canario, F. Machado, M. Soares, O. C. d'Almeida, M. Castelo-Branco, Simultaneous changes in visual acuity, cortical population receptive field size, visual field map size, and retinal thickness in healthy human aging. *Brain Struct. Funct.* (2021) https:/doi.org/10.1007/s00429-021-02338-0.

44. C. Song, D. S. Schwarzkopf, G. Rees, Variability in visual cortex size reflects tradeoff between local orientation sensitivity and global orientation modulation. *Nat. Commun.* **4**, 2201 (2013).

45. J. W. Kurzawski, D. G. Pelli, J. A. Winawer, Conservation across individuals of cortical crowding distance in human V4. *J. Vis.* **21**, 2675–2675 (2021).

46. B. M. Harvey, S. O. Dumoulin, The relationship between cortical magnification factor and population receptive field size in human visual cortex: constancies in cortical architecture. *Journal of Neuroscience* **31**, 13604–13612 (2011).

47. J. Abrams, A. Nizam, M. Carrasco, Isoeccentric locations are not equivalent: the extent of the vertical meridian asymmetry. *Vision Res.* **52**, 70–78 (2012).

48. A. S. Baldwin, T. S. Meese, D. H. Baker, The attenuation surface for contrast sensitivity has the form of a witch's hat within the central visual field. *J. Vis.* **12** (2012).

49. D. Regan, K. I. Beverley, Visual fields described by contrast sensitivity, by acuity, and by relative sensitivity to different orientations. *Invest. Ophthalmol. Vis. Sci.* **24**, 753–759 (1983).

50. M. F. Silva, S. Maia-Lopes, C. Mateus, M. Guerreiro, J. Sampaio, P. Faria, M. Castelo-Branco, Retinal and cortical patterns of spatial anisotropy in contrast sensitivity tasks. *Vision Res.* **48**, 127–135 (2008).

51. J. Rovamo, V. Virsu, An estimation and application of the human cortical magnification factor. *Exp. Brain Res.* **37**, 495–510 (1979).

52. J. G. Robson, N. Graham, Probability summation and regional variation in contrast sensitivity across the visual field. *Vision Res.* **21**, 409–418 (1981).

53. J. E. Corbett, M. Carrasco, Visual performance fields: frames of reference. *PLoS One* **6**, e24470 (2011).

54. S. Fuller, R. Z. Rodriguez, M. Carrasco, Apparent contrast differs across the vertical meridian: visual and attentional factors. *J. Vis.* **8**, 16.1–16 (2008).

55. M. Carrasco, P. E. Williams, Y. Yeshurun, Covert attention increases spatial resolution with or without masks: Support for signal enhancement. *J. Vis.* **2**, 1351–1365 (2002).

56. C. P. Talgar, M. Carrasco, Vertical meridian asymmetry in spatial resolution: Visual and attentional factors. *Psychon. Bull. Rev.* **9**, 714–722 (2002).

57. M. Carrasco, A. M. Giordano, B. McElree, Temporal performance fields: Visual and attentional factors. *Vision Res.* **44**, 1351–1365 (2004).

58. L. Montaser-Kouhsari, M. Carrasco, Perceptual asymmetries are preserved in short-term memory tasks. *Atten. Percept. Psychophys.* **71**, 1782–1792 (2009).

59. C. Myers, M. Carrasco, Adolescents' and adults' sensitivity differs around the visual field. *J. Vis.* **20**, 873–873 (2020).

60. T. M. Dekker, D. S. Schwarzkopf, B. de Haas, M. Nardini, M. I. Sereno, Population receptive field tuning properties of visual cortex during childhood. *Dev. Cogn. Neurosci.* **37**, 100614 (2019).

61. C. A. Curcio, K. R. Sloan, R. E. Kalina, A. E. Hendrickson, Human photoreceptor topography. *J. Comp. Neurol.* **292**, 497–523 (1990).

62. H. Song, T. Y. P. Chui, Z. Zhong, A. E. Elsner, S. A. Burns, Variation of cone photoreceptor packing density with retinal eccentricity and age. *Invest. Ophthalmol. Vis. Sci.* **52**, 7376–7384 (2011).

63. C. A. Curcio, K. A. Allen, Topography of ganglion cells in human retina. *J. Comp. Neurol.* **300**, 5–25 (1990).

64. A. B. Watson, A formula for human retinal ganglion cell receptive field density as a function of visual field location. *J. Vis.* **14** (2014).

65. E. R. Kupers, N. C. Benson, M. Carrasco, J. Winawer, Radial asymmetries around the visual field: From retina to cortex to behavior. *bioRxiv* (2020) https:/doi.org/10.1101/2020.10.20.347492.

66. M. M. Taylor, C. D. Creelman, PEST: Efficient Estimates on Probability Functions. *J. Acoust. Soc. Am.* **41**, 782–787 (1967).

67. A. Michelson, *Studies in Optics* (University of Chicago Press, 1927).

68. S. O. Dumoulin, B. A. Wandell, Population receptive field estimates in human visual cortex. *Neuroimage* **39**, 647–660 (2008).

69. M. Kleiner, D. H. Brainard, D. G. Pelli, C. Broussard, T. Wolf, D. Niehorster, What's new in Psychtoolbox-3? *Perception* (2007).

70. N. C. Benson, *et al.*, The Human Connectome Project 7 Tesla retinotopy dataset: Description and population receptive field analysis. *J. Vis.* **18**, 1–22 (2018).

71. N. Kriegeskorte, M. Mur, P. Bandettini, Representational similarity analysis - connecting the branches of systems neuroscience. *Front. Syst. Neurosci.* **2**, 4 (2008).

72. J. Xu, *et al.*, Evaluation of slice accelerations using multiband echo planar imaging at 3T. *Neuroimage* **83**, 991–1001 (2013).

73. D. A. Feinberg, *et al.*, Multiplexed echo planar imaging for sub-second whole brain fmri and fast diffusion imaging. *PLoS One* **5** (2010).

74. O. Esteban, *et al.*, fMRIPrep: a robust preprocessing pipeline for functional MRI. *Nat. Methods* **16**, 111–116 (2019).

75. K. Gorgolewski, *et al.*, Nipype: A flexible, lightweight and extensible neuroimaging data processing framework in Python. *Front. Neuroinform.* **5** (2011).

76. Y. Zhang, M. Brady, S. Smith, Segmentation of brain MR images through a hidden Markov random field model and the expectation-maximization algorithm. *IEEE Trans. Med. Imaging* **20**, 45–57 (2001).

77. A. M. Dale, B. Fischl, M. I. Sereno, Cortical surface-based analysis: I. Segmentation and surface reconstruction. *Neuroimage* (1999) https:/doi.org/10.1006/nimg.1998.0395.

78. K. J. Friston, *et al.*, Event-Related fMRI: Characterizing Differential Responses. *Neuroimage* **7**, 30–40 (1998).

79. K. J. Worsley, *et al.*, A general statistical analysis for fMRI data. *Neuroimage* **15**, 1–15 (2002).

80. N. C. Benson, J. Winawer, Bayesian analysis of retinotopic maps. *Elife* **7**, 1–29 (2018).

81. M. M. Schira, C. W. Tyler, M. Breakspear, B. Spehar, The foveal confluence in human visual cortex. *Journal of Neuroscience* **29**, 9050–9058 (2009).

Supplementary Information

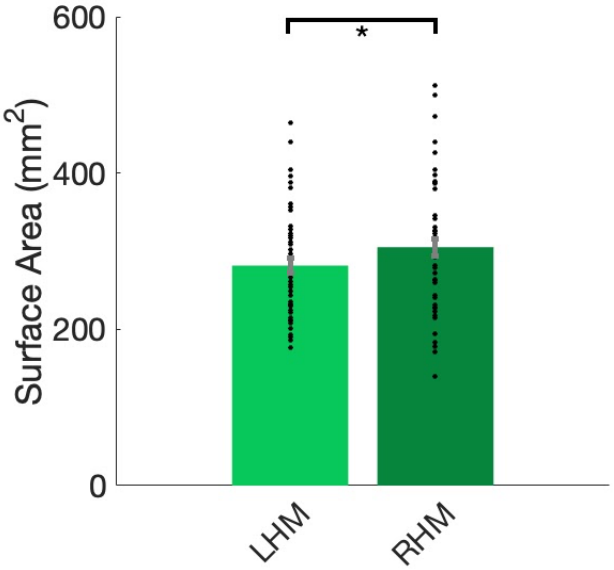

Figure S1. There is a slight bias towards more surface area dedicated to processing ±15° along the right horizontal meridian when compared to the left horizontal meridian ($t(53) = 2.06$, $p < .05$, $d = .28$). Data come from an extended dataset of 54 observers (29 included in the initial analysis and 25 additional observers). Error bars represent ±1 SEM.

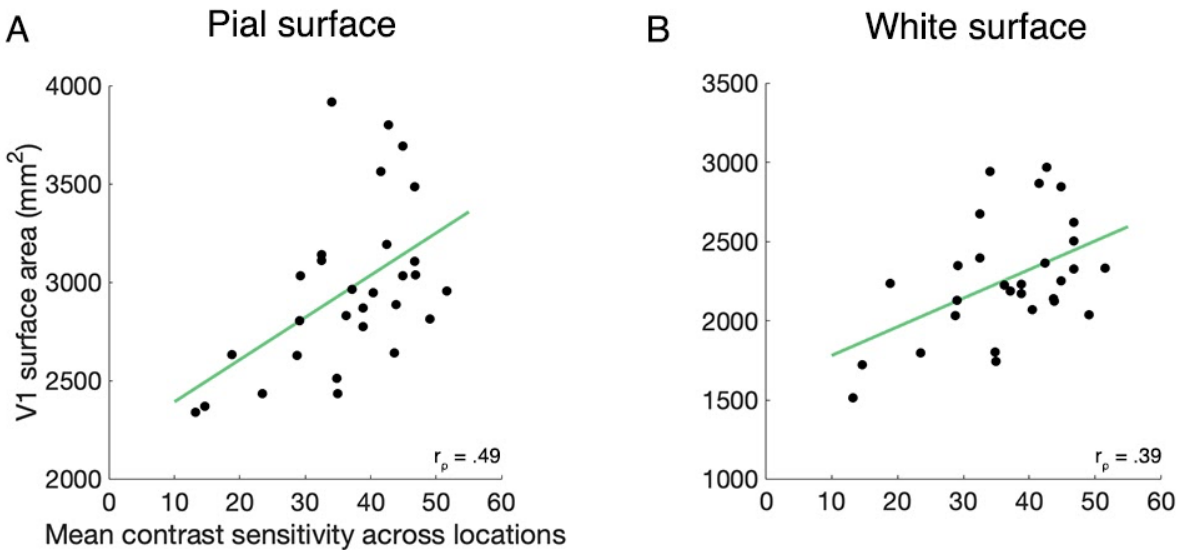

Figure S2. Average contrast sensitivity across polar angle locations correlates with **(A)** V1 pial surface area ($r_\rho = .49$, $p < .005$) and (B) V1 white matter surface area ($r_\rho = .39$, $p < .05$) (n=29).

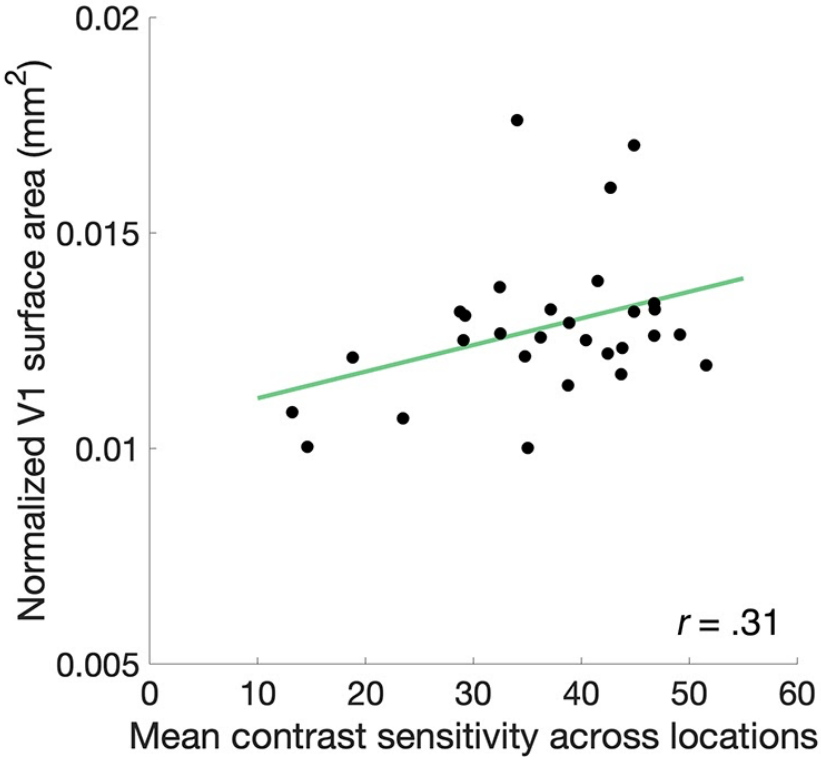

Figure S3. The correlation between average contrast sensitivity across polar angle locations and V1 surface area is reduced after normalizing V1 surface area to cortical surface area (r_ρ=.31, p=.53, n=29).

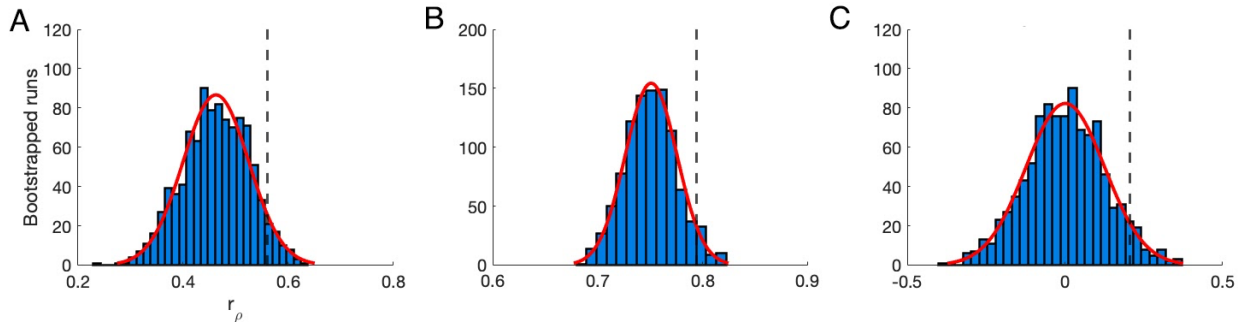

Figure S4. Histograms of the null distribution generated by bootstrapping 1000 Spearman's rho correlations. Each run shuffles the assignment of the four contrast sensitivity values and four local surface area values across observers and calculates Spearman's rho. The data in **(A)** correspond to the correlation in **Figure 4**, the data in **(B)** correspond to the correlation in **Figure 5A,** and the data in **(C)** correspond to the correlation in **Figure 5B**. The dashed black line indicates the r_ρ value at the 95th percentile; for **(A)** $x_{0.95} = .56$, for **(B)** $x_{0.95} = .79$, and **(C)** $x_{0.95} = .21$. The red line shows a normal distribution curve fit to the data.

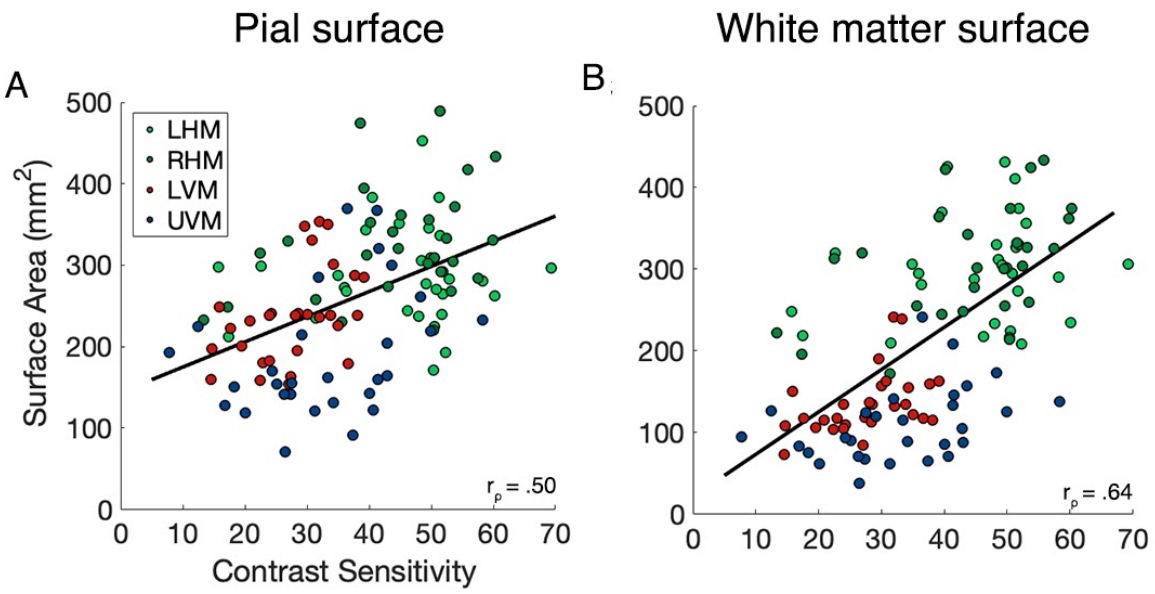

Figure S5. Local contrast sensitivity correlates with local V1 cortical magnification measurements (calculated using the **(A)** pial (r_ρ = .50, $x_{0.95}$ = .46) and **(B)** white matter surfaces (r_ρ = .64, $x_{0.95}$ = .57) taken from the corresponding meridians (n=29).

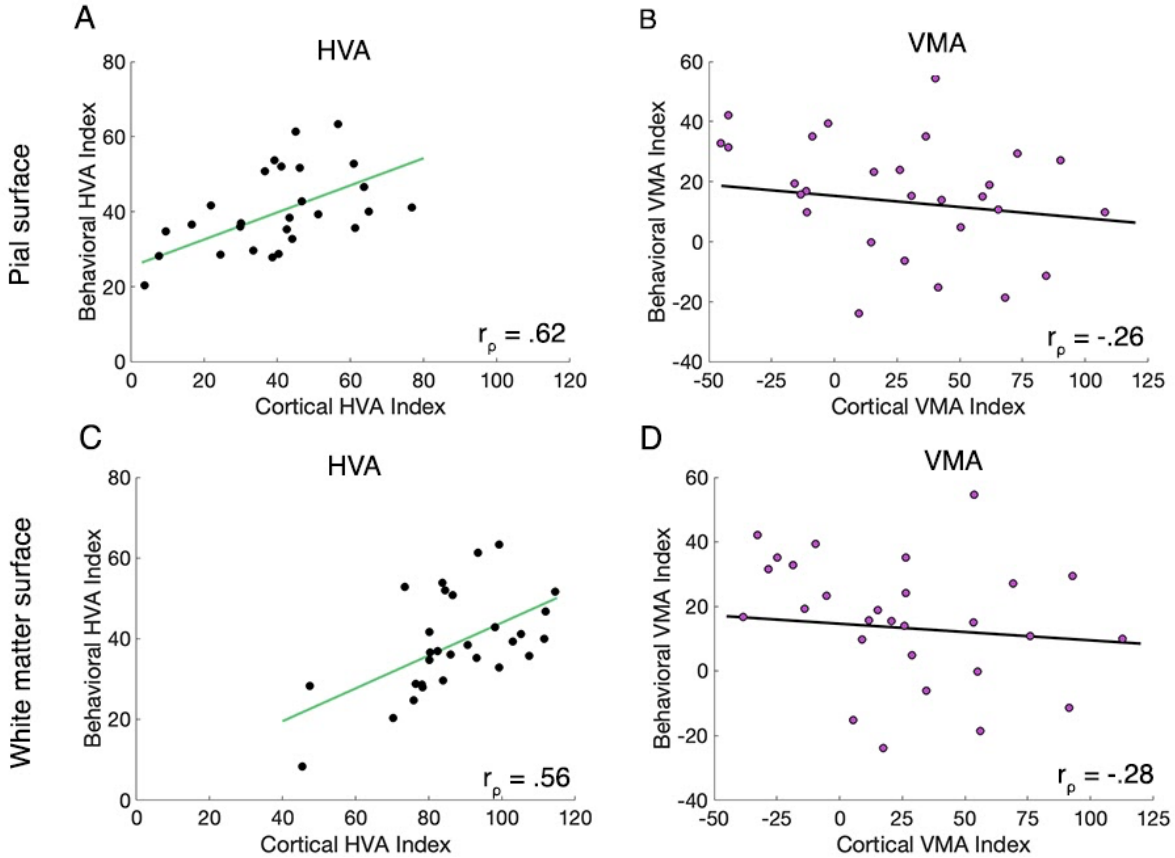

Figure S6. Behavioral and cortical HVA and VMA correlations. In **(A)** and **(B)** the cortical HVA and VMA are calculated using the pial surface in **(C)** and **(D)** they are calculated on the white matter surface. The behavioral and cortical HVA (pial surface) correlate, ($r_\rho = .62$, $p < .001$), as do the behavioral and cortical HVA (white matter surface) ($r_\rho = .56$, $p < .001$). The behavioral and cortical VMA (pial surface) do not correlate ($r_\rho = -.26$, $p > .1$), nor do the behavioral and cortical VMA (white matter surface) ($r_\rho = -.28$, $p > .1$).

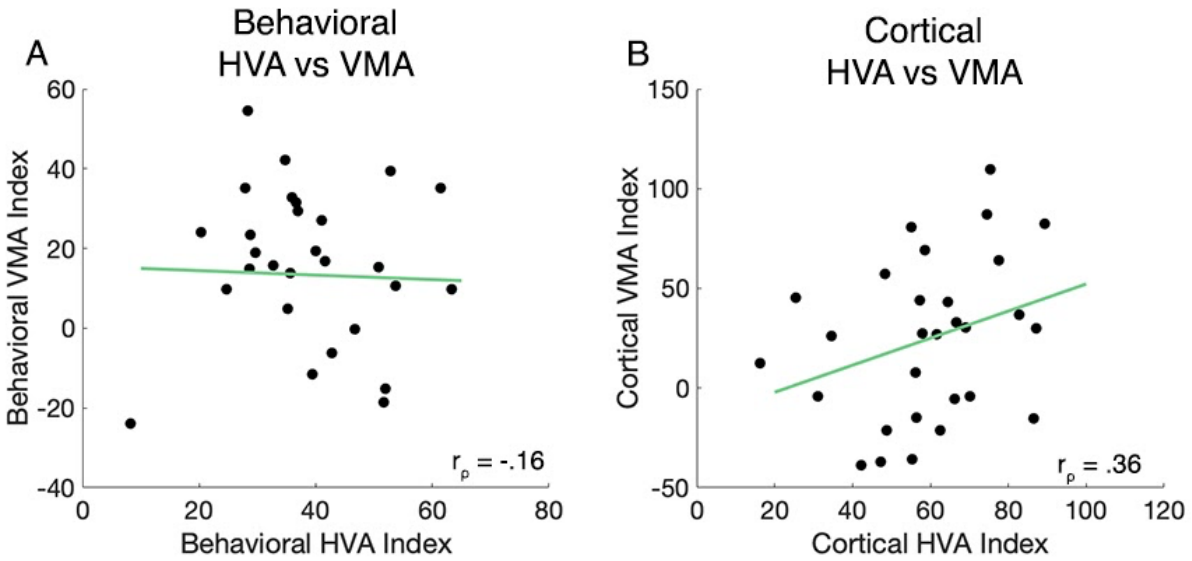

Figure S7. (A) The behavioral HVA and VMA are not correlated (r_ρ = -.16, p = .38), **(B)** the cortical HVA and VMA (r_ρ = .36, p =.05) are marginally correlated.